Ferroelectric, elastic, piezoelectric, and dielectric properties of $Ba(Ti_{0.7}Zr_{0.3})O_3$-$x(Ba_{0.82}Ca_{0.18})TiO_3$ Pb-free ceramics

Ruihao Yuan, Deqing Xue, Yumei Zhou, Xiangdong Ding, Jun Sun, and Dezhen Xue

Citation: Journal of Applied Physics **122**, 044105 (2017);
View online: https://doi.org/10.1063/1.4996353
View Table of Contents: http://aip.scitation.org/toc/jap/122/4
Published by the American Institute of Physics

Ferroelectric, elastic, piezoelectric, and dielectric properties of $Ba(Ti_{0.7}Zr_{0.3})O_3$-$x(Ba_{0.82}Ca_{0.18})TiO_3$ Pb-free ceramics

Ruihao Yuan, Deqing Xue, Yumei Zhou, Xiangdong Ding, Jun Sun, and Dezhen Xue[a)]
State Key Laboratory for Mechanical Behavior of Materials, Xi'an Jiaotong University, Xi'an 710049, China

(Received 13 May 2017; accepted 16 July 2017; published online 28 July 2017)

We designed and synthesized a pseudo-binary Pb-free system, $Ba(Ti_{0.7}Zr_{0.3})O_3$-$x(Ba_{0.82}Ca_{0.18})TiO_3$, by combining a rhombohedral end (with only cubic to rhombohedral ferroelectric phase transition) and a tetragonal end (with only cubic to tetragonal ferroelectric phase transition). The established composition-temperature phase diagram is characterized by a tricritical point type morphotropic phase boundary (MPB), and the MPB composition has better ferroelectric, piezoelectric, and dielectric properties than the compositions deviating from MPB. Moreover, a full set of material constants (including elastic stiffness constants, elastic compliance constants, piezoelectric constants, dielectric constants, and electromechanical coupling factors) of the MPB composition are determined using a resonance method. The good piezoelectric performance of the MPB composition can be ascribed to the high dielectric constants, elastic softening, and large electromechanical coupling factor. *Published by AIP Publishing*. [http://dx.doi.org/10.1063/1.4996353]

I. INTRODUCTION

Piezoelectric materials convert the mechanical strain into the electrical polarization (and vice versa).[1,2] They have found a wide range of applications, such as sensors, actuators, and transducers, especially in micro-electro-mechanical systems.[1,2] However, the Pb content in the current workhorse of Pb-based piezoelectric materials such as $Pb(Zr_xTi_{1-x})O_3$(PZT), $(1-x)Pb(Mg_{1/3}Nb_{2/3})O_3$-$xPbTiO_3$ (PMN-PT), and $(1-x)Pb(Zn_{1/3}Nb_{2/3})O_3$-$xPbTiO_3$ (PZN-PT) has caused serious environmental concern.[3–6] Thus, Pb-free alternatives are of great demand.[3–7]

Three perovskite systems including $(Bi,Na)TiO_3$-based, $(K,Na)NbO_3$-based, and $BaTiO_3$-based ceramics are the most promising Pb-free candidates.[6,8–12] In order to improve the piezoelectricity of those systems, various dopants are introduced into the host alloy to tailor the ferroelectric-ferroelectric phase transition temperature towards room temperature.[12,14–17] As a result, the instability of the polarization state at the transition temperature enhances the piezoelectricity. For example, Wu *et al.* doped Bi^{3+}, Sb^{5+}, Ba^{2+}, Zr^{4+}, and Hf^{4+} into $(K,Na)NbO_3$ to decrease the tetragonal to orthorhombic transition temperature of $(K,Na)NbO_3$ from 227 °C to room temperature, and the best composition with the tetragonal to orthorhombic phase transition at room temperature can exhibit a d_{33} of 570 pC/N.[18]

Another recipe for Pb-free piezoelectric materials is to build a morphotropic phase boundary (MPB) starting from a tricritical point in the composition-temperature phase diagram,[12,13] being analogous to the MPB in Pb-based systems, such as PZT.[1,19] Liu and Ren combined a Zr^{4+} stabilized rhombohedral end (with only cubic to rhombohedral ferroelectric phase transition) and a Ca^{2+} stabilized tetragonal end (with only cubic to tetragonal ferroelectric phase transition) to design a pseudo-binary Pb-free system, $Ba(Ti_{0.8}Zr_{0.2})O_3$ –$x(Ba_{0.7}Ca_{0.3})TiO_3$ (abbreviated as BZCTx).[12] The MPB composition, $Ba(Ti_{0.8}Zr_{0.2})O_3$ –50$(Ba_{0.7}Ca_{0.3})TiO_3$ (abbreviated as BZCT50), has a piezoelectric constant d_{33} of 620 pC/N.[12,20] Such a large piezoelectricity has been ascribed to an isotropically flattened energy profile at the MPB so that the polarization can be easily rotated by external stress or electric field.[12,21–23] The design strategy stimulates the occurrence of MPB in $Ba(Ti_{0.8}Hf_{0.2})O_3$–$x(Ba_{0.7}Ca_{0.3})TiO_3$ and $Ba(Ti_{0.88}Sn_{0.12})O_3$–$x(Ba_{0.7}Ca_{0.3})TiO_3$ pseudo-binary systems. Their MPB compositions show a d_{33} of more than 550 pC/N.[12,24,25]

Nevertheless, besides the above mentioned three systems, there are few systems with tricritical point type MPB designed following the strategy. Many efforts were devoted to searching for the high piezoelectricity in the $BaTiO_3$-based system by chemical modification of the BZCT50 prototype.[12,26–28] For example, Zhang *et al.* varied the Ca^{2+} concentration at the A-site while keeping the Zr^{4+} concentration unchanged in $(Ba_{1-x}Ca_x)(Ti_{0.95}Zr_{0.05})O_3$ and identified a d_{33} of 365 pC/N at $x = 0.08$.[26] Li *et al.* investigated the $(Ba_{0.95}Ca_{0.05})(Ti_{1-x}Zr_x)O_3$ system and showed a d_{33} of 338 pC/N at $x = 0.04$.[27] Besides, Sutapun *et al.* varied both Ca^{2+} and Zr^{4+} concentrations and found an optimized composition with d_{33} of 387 pC/N.[28] It seems that the simple composition scan is usually suboptimal in searching for high piezoelectricity, compared with the strategy of building a tricritical point type MPB.

In the present study, we thus designed and synthesized a pseudo-binary system with a MPB starting from a tricritical point. To avoid introducing complex multi-step phase transition, we combined a tetragonal end of $(Ba_{0.82}Ca_{0.18})TiO_3$, which only has a cubic to tetragonal phase transition, with a rhombohedral end of $Ba(Ti_{0.7}Zr_{0.3})O_3$, which only has a cubic to rhombohedral phase transition, to establish a $Ba(Ti_{0.7}Zr_{0.3})O_3$–$x(Ba_{0.82}Ca_{0.18})TiO_3$ system. We systematically investigated the ferroelectric, piezoelectric, and dielectric properties of the system, and we confirmed that the

[a)]Electronic mail: xuedezhen@mail.xjtu.edu.cn

properties at the MPB composition are superior to those at compositions deviating from MPB. We also determined all the material constants (including elastic stiffness constants, elastic compliance constants, piezoelectric constants, dielectric constants, and electromechanical coupling factors) of the MPB composition using a resonance method. The large piezoelectricity can be ascribed to the high dielectric constants, elastic softening, and large electromechanical coupling factor.

II. EXPERIMENT

All the ceramics were fabricated by a conventional solid-solid reaction method with raw materials of $BaCO_3$ (99.9%), $CaCO_3$ (99.9%), $BaZrO_3$ (99%), and TiO_2 (99.6%). Calcining and sintering were done at 1350 °C and 1450 °C for 3 h in air, respectively. The crystal structure of the samples was measured using powder X-ray diffraction (Shimadzu XRD-7000). The Curie temperature (T_C) and ferroelectric-ferroelectric phase transition temperatures (T_{T-O} and T_{O-R}) were determined from the dielectric permittivity (ε) versus temperature curves. Ferroelectric hysteresis loops were measured with a ferroelectric workstation at 10 Hz. The electrostrain was measured from disk samples under an electric field of 20 kV/cm using a MTI 2000 photonic sensor. The composition dependence of d_{33} was identified through a commercial Berlincourt-type d_{33} meter (ZJ-4AN) with poled pillar.

All samples for the resonance measurement were poled at room temperature (~20 °C) under an electric field of 1 kV/mm, and the frequency spectra were measured by using a HIOKI 3532–50 LCR meter. The poled ferroelectric ceramic has five elastic, three piezoelectric, and two dielectric independent constants. The free and clamped dielectric constants (ε_{11}^T, ε_{33}^T, ε_{11}^S, and ε_{33}^S), and the impermeability constants (β_{11}^T, β_{33}^T, β_{11}^S, and β_{33}^S) were detected from the low (1 kHz) and high frequency (twice of anti-resonance frequency) capacitances using the parallel-plate capacitor approximation. The elastic compliance constants (s_{33}^D, s_{33}^E, s_{11}^D, and s_{11}^E), the elastic stiffness constants (c_{33}^D, c_{33}^E, c_{44}^D, and c_{44}^E), and the electromechanical coupling factors (k_{33}, k_{31}, k_{15}, k_p, and k_t) were calculated from the resonance and anti-resonance frequencies of resonators with geometries defined in the IEEE standards.[29] After that, the piezoelectric strain coefficients (d_{33}, d_{31}, and d_{15}), the piezoelectric stress coefficients (e_{33}, e_{31}, and e_{15}), the piezoelectric voltage coefficients (g_{33}, g_{31}, and g_{15}), the piezoelectric stiffness coefficients (h_{33}, h_{31}, and h_{15}), and the rest of the elastic compliance and stiffness coefficients (s_{12}^D, s_{12}^E, s_{66}^D, s_{66}^E, c_{66}^D, c_{66}^E, s_{13}^D, s_{13}^E, c_{11}^E, c_{12}^E, c_{13}^E, c_{11}^D, c_{12}^D, and c_{13}^D) were derived from the measured properties.[20,29,30]

III. RESULTS AND DISCUSSION

A. A pseudo-binary phase diagram with a tricritical type MPB of $Ba(Ti_{0.7}Zr_{0.3})O_3$-$x(Ba_{0.82}Ca_{0.18})TiO_3$ Pb-free ceramics

In order to establish a phase diagram with a MPB starting from a tricritical point, we need to combine two end compounds which only have one step paraelectric to ferroelectric phase transition, i.e., from cubic to tetragonal or cubic to rhombohedral. We thus chose $(Ba_{0.82}Ca_{0.18})TiO_3$ (abbreviated as BCT) as our tetragonal end. The Ca^{2+} concentration is selected from the phase diagram of the $(Ba_{1-x}Ca_x)TiO_3$ system, which is indicated by the arrow in the inset of Fig. 1(a). Its dielectric permittivity (ε) versus temperature curve in Fig. 1(a) confirms that only one step phase transition occurs. Figure 1(b) shows the ε versus temperature curve of our rhombohedral end, $Ba(Ti_{0.7}Zr_{0.3})O_3$ (abbreviated as BZT), indicating that only one step phase transition from the cubic phase to the rhombohedral phase takes place. We chose the Zr^{4+} concentration from the phase diagram of $Ba(Ti_{1-x}Zr_x)O_3$, as shown by the arrow in the inset of Fig. 1(b).

Since the end compounds are determined, we combined them to synthesise a pseudo-binary solid solution to search for a tricritical point type MPB. The X-ray diffraction profiles of the system with 2θ ranging from 20° to 70° are presented in Fig. 2(a). All the samples show a typical perovskite structure. The ⟨200⟩ peak around 45° gradually splits into two peaks with increasing content of the BCT end, indicating a structural transformation from a pseudo-cubic phase to a tetragonal phase.[12,24,25] Lattice parameters of the structure were then calculated from the characteristic peak in Fig. 2(a), with a fine scan to determine the precise peak position. Figure 2(b) shows the lattice parameters (a_{pc}, a_T, and c_T) and tetragonality factor (c/a - 1) as a function of BCT end, x. The pseudo-cubic lattice parameter a_{pc} decreases with increasing BCT content. When the BCT content exceeds 70%, pseudo-cubic phase transforms into the tetragonal phase and the

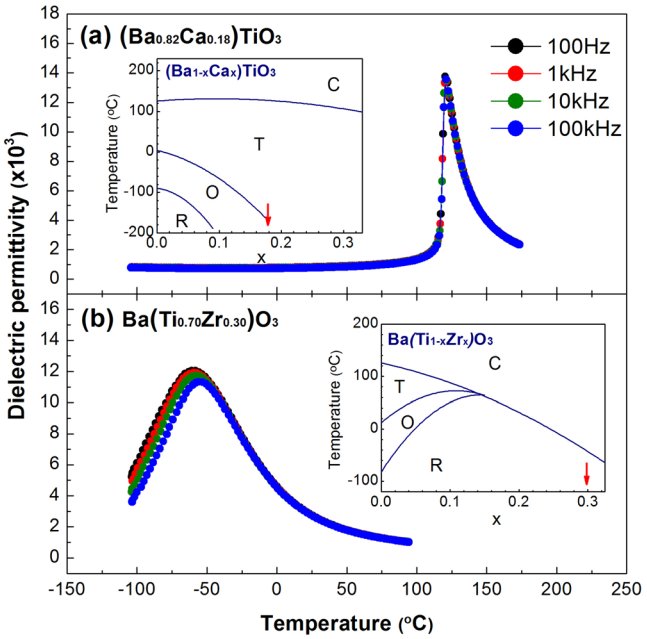

FIG. 1. The dielectric permittivity (ε) versus temperature curve at different frequencies of (a) the tetragonal end, $(Ba_{0.82}Ca_{0.18})TiO_3$, and (b) the rhombohedral end, $Ba(Ti_{0.7}Zr_{0.3})O_3$, of our designed pseudo-binary system. The inset of (a) shows the phase diagram of $(Ba_{1-x}Ca_x)TiO_3$ (Ref. 31) and the arrow in it indicates the composition of our tetragonal end. The inset of (b) shows the phase diagram of $Ba(Ti_{1-x}Zr_x)O_3$ (Ref. 32) and the arrow in it indicates the composition of our rhombohedral end.

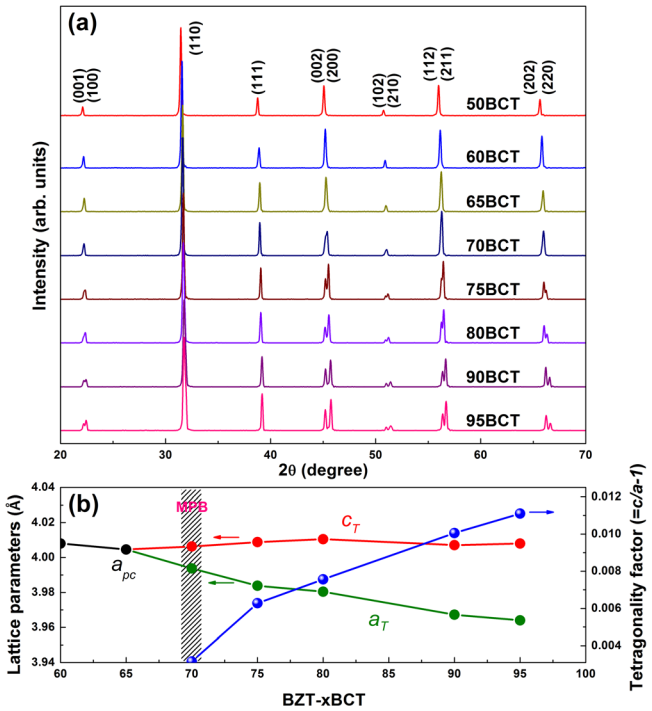

FIG. 2. (a) X-ray diffraction profile of BZT-xBCT ($x = 50$, 60, 65, 70, 75, 80, 90, and 95). (b) The lattice parameters and tetragonality factor as a function of BCT concentration (x). The possible morphotropic phase boundary between pseudo-cubic and tetragonal is at $x = 70$, as indicated by the shaded area. Solid lines are guides to the eye.

tetragonality factor of the tetragonal phase increases with BCT end, x.

A clear crystal structure change can be observed when the BCT content increases. We thus expect that there is a tricritical point type MPB in the composition-temperature phase diagram. Figure 3 shows ε as a function of temperature for different compositions. They are measured at a frequency of 1 kHz during cooling and within the temperature range

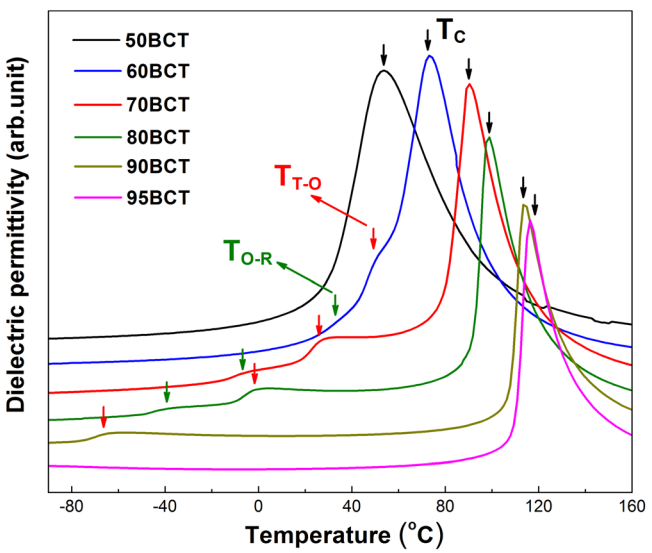

FIG. 3. The ε versus temperature curves of different compositions at a frequency of 1 kHz during cooling. The black, red, and green arrows indicate the cubic to tetragonal phase transition temperature(T_C), tetragonal to orthorhombic phase transition temperature (T_{T-O}), and orthorhombic to rhombohedral phase transition temperature (T_{O-R}), respectively.

from 160 °C to −85 °C. Only one peak can be observed at $x = 50$ and $x = 95$, indicating that only one step paraelectric to ferroelectric phase transition takes place in these two compositions. The phase transition of $x = 50$ is cubic to rhombohedral upon cooling, as it is close to the R end. The $x = 95$ composition transforms from cubic to tetragonal upon cooling, as it is close to the T end. Besides, three peaks appear when x is equal to 60, 70, and 80. The first peak corresponds to the C-T phase transition temperature (T_C, as shown by the black arrows in Fig. 3), while the latter two peaks correspond to the T-O and O-R phase transition temperatures, respectively (T_{T-O} and T_{O-R}, as shown by the red and green arrows in Fig. 3).[33–35] Only two peaks appear at $x = 90$, which are T_C and T_{T-O}. The absence of T_{O-R} is because the transition temperature is too low to be detected.

The presence of an intermediate phase (O phase here) is in consistence with the recent studies on the BZCT50 prototype system.[33,34] The high resolution X-ray diffraction results suggest a single O phase bridging the T and R phases,[33] and several TEM studies have shown that the local structure of such an intermediate phase can be considered as a nano-scale adaptive phase of nanoregions with T and R symmetries.[33,36–38] As there is no group-subgroup relationship between the T and R symmetries, the purpose of the presence of an orthorhombic phase is to let a smooth transformation between the T phase and the R phase. Thus, two separate boundaries can be observed, i.e., T-O and O-R. The T-O phase boundary is shown to have a better piezoelectricity than the O-R phase boundary. Such a superior performance is attributed to the more significant elastic softening at the T-O phase boundary than that at the O-R phase boundary, as shown by the dynamic mechanical analysis.[34] For the prototype BZCT50, the T-O phase boundary locates just around room temperature (∼20 °C) and thus a very small elastic stiffness constant is expected.[12,20] However, the T-O phase boundary in our BZT-70BCT is higher than room temperature, which presumably results in a larger elastic stiffness constant of BZT-70BCT at room temperature. A larger elastic stiffness constant should occur in pure $BaTiO_3$ as well, as its T-O phase boundary is lower than room temperature.[32]

With the T_C, T_{T-O}, and T_{O-R} transition temperatures determined from the ε versus temperature curves in Fig. 3, the phase diagram of the new BZT-xBCT system was established, as shown in Fig. 4. The phase diagram is divided into four regions of C, T, O, and R phases by three phase boundaries. The T-O and O-R phase boundaries start from a C-T-O-R quasi-quadruple point located at $x = 51$ and at $T = 57$ °C. The inset of Fig. 4 shows the thermal hysteresis of C-T, C-R, and T-O phase transitions, which are calculated from the ε versus temperature curves upon heating and cooling. The thermal hysteresis of the T-O transition decreases sharply towards the quasi-quadruple point and nearly vanishes at this point. The thermal hysteresis of C-T and C-R transitions also shows similar tendency of decreasing towards the quasi-quadruple point. Such facts suggest that this quasi-quadruple point is likely to be a tricritical point corresponding to a crossover from a discontinuous to a continuous transition. The similar behavior has been found in

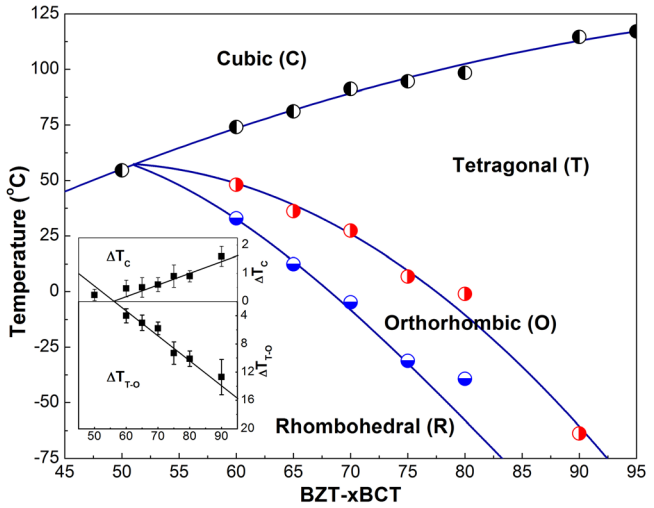

FIG. 4. Composition-temperature phase diagram of BZT-*x*BCT. The inset figure shows the thermal hysteresis of the *C-T*, *C-R*, and *T-O* phase transition, and nearly zero thermal hysteresis takes place around the quasi-quadruple point, indicating that it is a tricritical point.

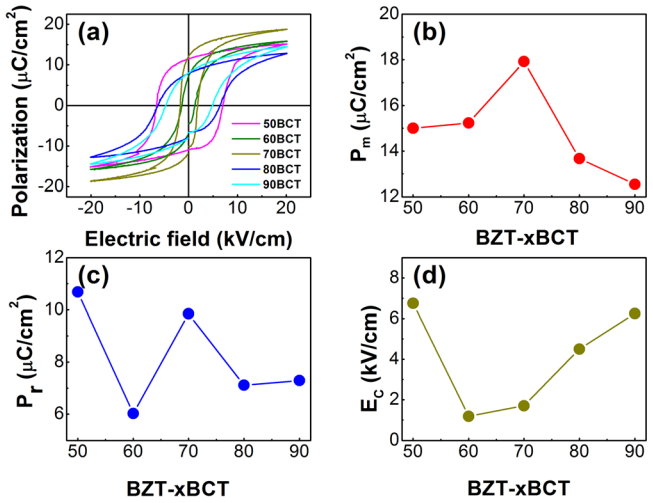

FIG. 5. (a) The polarization (P) versus electric field (E) curves of BZT-*x*BCT ($x = 50$, 60, 70, 80, and 90). (b) The saturation polarization P_m as a function of BCT content, x. (c) The remnant polarization P_r as a function of BCT content, x. (d) The coercive field E_c as a function of BCT content, x. An anomaly can be found at $x = 70$.

other tricritical point MPB systems,[12,24,25] in which zero hysteresis occurs near the triple or quasi-quadruple point.

The phase transition at the MPB leads to a large instability in the polarization state, and a significant variation of the polarization can be induced by external stress or electric field. More importantly, such a MPB originates from a tricritical point. The continuous nature of the transition at the tricritical point allows the free energy landscape to be more isotropically flattened with respect to polarization states.[12,21–23] Consequently, the intrinsic polarization rotation and extension and even the extrinsic domain wall contribution and the elastic softening may lead to anomalies in the ferroelectric, piezoelectric, and dielectric properties at the MPB composition.[21,39,40]

B. Ferroelectric, piezoelectric, and dielectric properties of $Ba(Ti_{0.7}Zr_{0.3})O_3$–$x(Ba_{0.82}Ca_{0.18})TiO_3$ Pb-free ceramics

In this subsection, the ferroelectric, piezoelectric, and dielectric properties of $Ba(Ti_{0.7}Zr_{0.3})O_3$–$x(Ba_{0.82}Ca_{0.18})TiO_3$ Pb-free ceramics as a function of BCT content x were investigated. Figure 5(a) plots the polarization (P) versus electric field (E) hysteresis loops at room temperature (~20 °C) for different compositions. These P–E hysteresis loops show typical ferroelectric features. It evolves from a fat one, through a rawboned one and then back to fat one with increasing BCT content. Figures 5(b)–5(d) summarize the composition dependence of the saturation polarization P_m, remnant polarization P_r, and coercive field E_c, respectively. All the properties show anomalies at $x = 70$, specifically, the large value of P_m, P_r, and fairly low E_c. This is in consistence with our expectation and may hint anomalous piezoelectric properties.

Figure 6(a) shows ε at room temperature (~20 °C) as a function of BCT content, x. The dielectric permittivity of the MPB composition, $x = 70$, is about 3300, comparable with that of soft PZT materials (2000–3500)[3] and the BZCT50 prototype system (~3800).[12] It has been shown that $\varepsilon_r P_r$ is closely related to the piezoelectric properties.[34] We thus plotted $\varepsilon_r P_r$ as a function of composition x in Fig. 6(b). An anomaly is shown at the MPB composition.

Figure 7 reveals the composition dependence of piezoelectric properties of the $Ba(Ti_{0.7}Zr_{0.3})O_3$–$x(Ba_{0.82}Ca_{0.18})TiO_3$ Pb-free ceramics. The strain (S) versus electric field (E) curves are presented in Fig. 7(a). They are all typical butterfly-like electro-strain curves. The maximum strain at 20 kV/cm is plotted as a function of x in Fig. 7(b). A high value of 0.12% occurs at $x = 70$. The S_{max}/E_{max}, as shown in Fig. 7(c), exhibits the highest value of 605 pm/V at BZT-70BCT. The high value is smaller than that of the soft PZT ceramics (900 pm/V) and prototype system BZCT50 (1140 pm/V), which is measured in a smaller field of 500 V/mm.[12] The electrostrictive coefficient Q_{33} of BZT-*x*BCT ceramics was obtained by fitting the electro-strain (S) versus

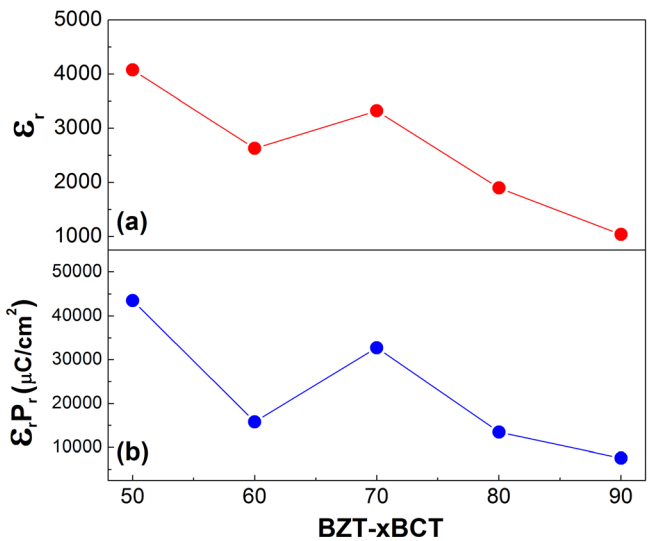

FIG. 6. (a) The ε_r at room temperature and the $\varepsilon_r P_r$ as a function of BCT content, x.

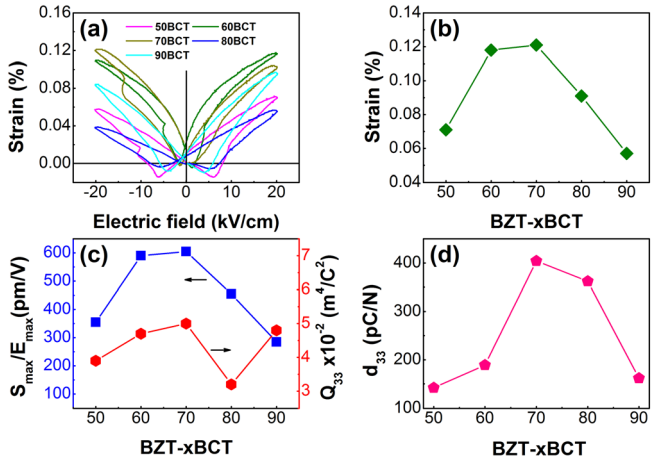

FIG. 7. (a) The strain (S) versus electric field (E) curves of BZT-xBCT ($x = 50$, 60, 70, 80, and 90). (b) The strain (S) under the electric field of 20 kV/cm as a function of BCT content, x. (c) The S_{max}/E_{max} and Q_{33} as a function of BCT content, x. (d) The d_{33} value measured by the Berlincourt-type meter as a function of BCT content, x. The anomaly can be found at $x = 70$.

polarization (P) curves with $S = Q_{33}P^2$. The composition dependence of Q_{33} is plotted in Fig. 7(c). The best Q_{33} of 0.05 m^4/C^2 occurs at the composition $x = 70$. It is larger than that of the BZCT50 prototype, which is reported to be about 0.045 m^4/C^2.[41] The d_{33} measured by the Berlincourt-type d_{33} meter as a function of composition is shown in Fig. 7(d). It shows a maximum about 420 pC/N for $x = 70$ and decreases when the composition deviates from the 70BCT. But it still maintains 380 pC/N for $x = 80$.

The property anomaly is analogous to that found in BZCT50 prototype[12] and Pb-based PZT,[42] PMN-PT,[42,43] and PZN-PT[44] systems. Therefore, establishing a MPB starting from a tricritical point in a pseudo-binary temperature-composition phase diagram can be a promising recipe to enhance the piezoelectricity.

C. Material constants of Ba(Ti$_{0.7}$Zr$_{0.3}$)O$_3$–70 (Ba$_{0.82}$Ca$_{0.18}$)TiO$_3$ Pb-free ceramic

We obtained a large d_{33} at the MPB composition, $x = 70$. Although the d_{33} value is larger than that of compositions away from MPB, it is still smaller than the value of the BZCT50 prototype.[12] To understand the reason of the deviation, we determined a complete set of elastic, dielectric, and piezoelectric constants (tensor components) of the Ba(Ti$_{0.7}$Zr$_{0.3}$)O$_3$–70(Ba$_{0.82}$Ca$_{0.18}$)TiO$_3$ ceramic of the MPB composition at room temperature (~20 °C) by using a resonance method. All these properties were compared to the pure BaTiO$_3$ ceramic, soft PZT ceramic (PZT5A), and prototype BZCT50 ceramic. Moreover, such a dataset is indispensable for device design based on the material and also for further theoretical studies.

Table I lists the elastic stiffness constants and elastic compliance constants of the MPB composition. Those of pure BaTiO$_3$ ceramic,[45] BZCT50,[24] and PZT5A[30] are also included. It can be seen that elastic stiffness constants, c_{11}^D, c_{33}^D, c_{44}^D, c_{66}^D, c_{33}^E, c_{44}^E, and c_{66}^E, are smaller or softer than those of the pure BaTiO$_3$ ceramic and are comparable to those of BZCT50 and PZT5. Elastic compliance constants, s_{11}^D, s_{44}^D, s_{66}^D, s_{11}^E, s_{12}^E, s_{44}^E, and s_{66}^E, are adjacent to those of BZCT50 and PZT5A. The values of other elastic constants are between the values of pure BaTiO$_3$ and BZCT50. This may be a reason that our MPB composition has superior piezoelectric performance than the pure BaTiO$_3$ but inferior performance than the BZCT50.

Table II lists piezoelectric coefficients, dielectric constants, and electromechanical coupling factors of BZT-70BCT and shows the comparison to those of pure BaTiO$_3$ ceramic,[45] BZCT50,[24] and PZT5A[30] ceramic. The d_{33} value of our MPB composition is higher than that of PZT5A but is smaller than that of BZCT50. Interestingly, the piezoelectric coefficients of e_{33} and h_{33} have a better value than those of BZCT50. The dielectric constants, ε_{ij}, of our MPB composition are not as large as those of BZCT50 but are much higher than those of PZT5A, whereas the electromechanical coupling factors are smaller than those of BZCT50 and PZT5A, except that the k_{33} value is comparable with that of BZCT50. It is known that the piezoelectric coefficient d_{ij} could be expressed as

$$d_{ij} = (k_{ij}^2 \varepsilon_{ij} s_{jj})^{0.5}. \quad (1)$$

TABLE I. Measured and derived elastic constants of the poled Ba(Ti$_{0.7}$Zr$_{0.3}$)O$_3$-70(Ba$_{0.82}$Ca$_{0.18}$)TiO$_3$ ceramic compared with BaTiO$_3$ ceramic,[45] BZCT50 (Ref. 24), and PZT5A ceramic.[30] c_{ij} (10^{10} N/m^2) and s_{ij} (10^{-12} m^2/N) represent the elastic stiffness constants and elastic compliance constants, respectively.

	Elastic Stiffness Constants, c_{ij} (10^{10} N/m^2)											
Material	c_{11}^D	c_{12}^D	c_{13}^D	c_{33}^D [a]	c_{44}^D [a]	c_{66}^D	c_{11}^E	c_{12}^E	c_{13}^E	c_{33}^E [a]	c_{44}^E [a]	c_{66}^E
BZT-70BCT	11.7	6.6	2.2	13.9	3.07	2.65	10.4	5.3	3.1	12.4	2.95	2.65
BaTiO$_3$	16.8	7.82	7.10	18.9	5.46	4.48	16.6	7.66	7.75	16.2	4.29	4.28
BZCT50	13.7	9.0	8.0	13.7	3.44	2.44	13.6	8.9	8.5	11.3	2.66	2.44
PZT5A	12.6	8.1	6.5	14.7	4.0	2.3	12.1	7.7	7.7	11.1	2.1	2.3
	Elastic Compliance Constants, s_{ij} (10^{-12} m^2/N)											
	s_{11}^D [a]	s_{12}^D	s_{13}^D	s_{33}^D [a]	s_{44}^D	s_{66}^D	s_{11}^E [a]	s_{12}^E	s_{13}^E	s_{33}^E [a]	s_{44}^E	s_{66}^E
BZT-70BCT	13.2	−5.7	−2.7	9.2	32.6	37.8	13.7	−5.2	−4.2	15.0	33.8	37.8
$BaTiO_3$	8.18	−2.98	−1.95	6.76	18.3	22.3	8.55	−2.61	−2.85	8.93	23.3	22.3
BZCT50	14.0	−7.0	−3.8	11.4	29.1	42.0	15.5	−5.5	−7.4	19.7	37.6	42.0
PZT5A	14.4	−7.7	−3.0	9.5	25.2	44.3	16.4	−5.8	−7.3	18.8	47.5	44.3

[a]Directly measured properties.

TABLE II. Measured and derived piezoelectric, dielectric, and electromechanical constants of the poled $Ba(Ti_{0.7}Zr_{0.3})O_3$-70$(Ba_{0.82}Ca_{0.18})TiO_3$ ceramic compared with the $BaTiO_3$ ceramic,[45] BZCT50 (Ref. 24) and PZT5A ceramic.[30] d_{ij} (pC/N), e_{ij} (C/m^2), g_{ij} (10^{-3} Vm/N), and h_{ij} (10^8 V/m) represent the piezoelectric constants, ε_{ij} (ε_0) and β_{ij} ($10^{-4}/\varepsilon_0$) are the dielectric constants, and k_{ij} correspond to electromechanical coupling factors.

	Piezoelectric Constants												
	d_{ij}(pC/N)				e_{ij}(C/m^2)			g_{ij}(10^{-3} Vm/N)			h_{ij}(10^8 V/m)		
Material	d_{33}	d_{31}	d_{15}	d_{33}[a]	e_{33}	e_{31}	e_{15}	g_{33}	g_{31}	g_{15}	h_{33}	h_{31}	h_{15}
BZT-70BCT	410	−120	195	420	43.4	−6.1	5.8	12.5	−3.7	19.8	14.7	−2.1	2.4
$BaTiO_3$	191	−79	270	190	11.6	−4.4	18.6	11.4	−4.7	18.8	9.2	−3.5	16.6
BZCT50	546	−231	453	620	22.4	−5.7	12.1	15.3	−6.5	31.0	8.6	−2.1	8.3
PZT5A	374	−171	584	410	15.8	−5.4	12.3	24.9	−11.4	38.0	21.4	−7.3	15.0

	Dielectric Constants								Electromechanical Coupling Factors				
	$\varepsilon_{ij}(\varepsilon_0)$				$\beta_{ij}(10^{-4}/\varepsilon_0)$								
	ε_{33}^{T}[a]	ε_{11}^{T}[a]	ε_{33}^{S}[a]	ε_{11}^{S}[a]	β_{33}^{T}	β_{11}^{T}	β_{33}^{S}	β_{11}^{S}	k_{33}	k_{31}	k_{15}	k_t	k_p
BZT-70BCT	3272	3266	2956	2416	3.06	3.06	3.38	4.14	0.62	0.19	0.20	0.32	0.41
$BaTiO_3$	1898	1622	1419	1269	5.3	6.2	7.0	7.9	0.49	0.21	0.48	…	0.35
BZCT50	4050	2732	2930	1652	2.47	3.66	3.41	6.05	0.65	0.31	0.48	0.42	0.53
PZT5A	1700	1730	830	916	5.9	5.8	12.0	10.9	0.70	0.34	0.68	0.49	0.60

[a]Directly measured properties.

As listed in Tables I and II, k_{33}, s_{33}, and ε_{33} of our MPB composition are smaller than those of BZCT50. According to Eq. (1), our MPB composition is not as good as BZCT50 in terms of d_{33}. But ε_{33} of our MPB composition is much larger than that of PZT5A, even though k_{33} and s_{33} are relatively smaller. As a result, our MPB composition has a larger d_{33} than PZT5A.

IV. SUMMARY

In summary, by combining a Zr^{4+} stabilized rhombohedral end (with only cubic to rhombohedral ferroelectric phase transition) and a Ca^{2+} stabilized tetragonal end (with only cubic to tetragonal ferroelectric phase transition), we designed a pseudo-binary Pb-free system, $Ba(Ti_{0.7}Zr_{0.3})O_3$ $-x(Ba_{0.82}Ca_{0.18})TiO_3$, with a tricritical type MPB. We confirmed that the MPB composition has better ferroelectric, piezoelectric, and dielectric properties than the compositions deviating from MPB. Moreover, a full set of material constants (including elastic stiffness constants, elastic compliance constants, piezoelectric constants, dielectric constants, and electromechanical coupling factors) of the MPB composition are determined using a resonance method.

ACKNOWLEDGMENTS

The authors gratefully acknowledge the support of the National Natural Science Foundation of China (Grant Nos. 51571156, 51671157, 51302209, 51621063, 51431007, and 51320105014), and Program for Changjiang Scholars and Innovative Research Team in University (IRT13034).

[1]B. Jaffe, *Piezoelectric Ceramics* (Elsevier, 2012), Vol. 3.
[2]K. Uchino, *Ferroelectric Devices* (Marcel Dekker, New York, 2000).
[3]T. R. Shrout and S. J. Zhang, "Lead-free piezoelectric ceramics: Alternatives for PZT?," J. Electroceram. **19**, 113–126 (2007).
[4]T. Takenaka, H. Nagata, and Y. Hiruma, "Current developments and prospective of lead-free piezoelectric ceramics," Jpn. J. Appl. Phys., Part 1 **47**, 3787 (2008).
[5]Y. Saito, H. Takao, T. Tani, T. Nonoyama, K. Takatori, T. Homma, T. Nagaya, and M. Nakamura, "Lead-free piezoceramics," Nature **432**, 84–87 (2004).
[6]J. Rödel, W. Jo, K. T. P. Seifert, E.-M. Anton, T. Granzow, and D. Damjanovic, "Perspective on the development of lead-free piezoceramics," J. Am. Ceram. Soc. **92**, 1153–1177 (2009).
[7]N. Setter, D. Damjanovic, L. Eng, G. Fox, S. Gevorgian, S. Hong, A. Kingon, H. Kohlstedt, N. Y. Park, G. B. Stephenson, I. Stolitchnov, A. K. Taganstev, D. V. Taylor, T. Yamada, and S. Streiffer, "Ferroelectric thin films: Review of materials, properties, and applications," J. Appl. Phys. **100**, 051606 (2006).
[8]W. Jo, J. E. Daniels, J. L. Jones, X. Tan, P. A. Thomas, D. Damjanovic, and J. Rödel, "Evolving morphotropic phase boundary in lead-free $(Bi_{1/2}Na_{1/2})TiO_3$-$BaTiO_3$ piezoceramics," J. Appl. Phys. **109**, 014110 (2011).
[9]C. Ma, X. Tan, E. Dul'kin, and M. Roth, "Domain structure-dielectric property relationship in lead-free (1-x)$(Bi_{1/2}Na_{1/2})TiO_3$-x$BaTiO_3$ ceramics," J. Appl. Phys. **108**, 104105 (2010).
[10]C.-W. Ahn, C.-S. Park, C.-H. Choi, S. Nahm, M.-J. Yoo, H.-G. Lee, and S. Priya, "Sintering behavior of lead-free (K,Na)NbO_3-based piezoelectric ceramics," J. Am. Ceram. Soc. **92**, 2033–2038 (2009).
[11]K. Wang and J.-F. Li, "Domain engineering of lead-free Li-modified (K,Na)NbO_3 polycrystals with highly enhanced piezoelectricity," Adv. Funct. Mater. **20**, 1924–1929 (2010).
[12]W. Liu and X. Ren, "Large piezoelectric effect in Pb-free ceramics," Phys. Rev. Lett. **103**, 257602 (2009).
[13]D. Xue, P. V. Balachandran, R. Yuan, T. Hu, X. Qian, E. Dougherty, and T. Lookman, "Accelerated search for batio$_3$-based piezoelectrics with vertical morphotropic phase boundary: Synthesis guided by learning," Proc. Natl. Acad. Sci. U.S.A. **113**, 13301–13306 (2016).
[14]X. Wang, J. Wu, D. Xiao, J. Zhu, X. Cheng, T. Zheng, B. Zhang, X. Lou, and X. Wang, "Giant piezoelectricity in potassium-sodium niobate lead-free ceramics," J. Am. Chem. Soc. **136**, 2905–2910 (2014).
[15]J. Wu, D. Xiao, and J. Zhu, "Potassium-sodium niobate lead-free piezoelectric materials: Past, present, and future of phase boundaries," Chem. Rev. **115**, 2559–2595 (2015).
[16]S. Zhang, T. R. Shrout, H. Nagata, Y. Hiruma, and T. Takenaka, "Piezoelectric properties in $(K_{0.5}Bi_{0.5})TiO_3$-$(Na_{0.5}Bi_{0.5})TiO_3$-$BaTiO_3$ lead-free ceramics," IEEE Trans. Ultrason., Ferroelectr., Freq. Control **54**, 910–917 (2007).
[17]B.-J. Chu, D.-R. Chen, G.-R. Li, and Q.-R. Yin, "Electrical properties of $Na_{1/2}Bi_{1/2}TiO_3$-$BaTiO_3$ ceramics," J. Eur. Ceram. Soc. **22**, 2115–2121 (2002).

[18]K. Xu, J. Li, X. Lv, J. Wu, X. Zhang, D. Xiao, and J. Zhu, "Superior piezoelectric properties in potassium-sodium niobate lead-free ceramics," Adv. Mater. **28**, 8519–8523 (2016).
[19]B. Jaffe, R. Roth, and S. Marzullo, "Properties of piezoelectric ceramics in the solid-solution series lead titanate-lead zirconate-lead oxide: Tin oxide and lead titanate-lead hafnate," J. Res. Natl. Bur. Stand. **55**, 239–254 (1955).
[20]D. Xue, Y. Zhou, H. Bao, C. Zhou, J. Gao, and X. Ren, "Elastic, piezoelectric, and dielectric properties of $Ba(Zr_{0.2}Ti_{0.8})O_3$-50$(Ba_{0.7}Ca_{0.3})TiO_3$ Pb-free ceramic at the morphotropic phase boundary," J. Appl. Phys. **109**, 054110 (2011).
[21]D. Damjanovic, "A morphotropic phase boundary system based on polarization rotation and polarization extension," Appl. Phys. Lett. **97**, 062906 (2010).
[22]J. Gao, L. Zhang, D. Xue, T. Kimoto, M. Song, L. Zhong, and X. Ren, "Symmetry determination on Pb-free piezoceramic 0.5$Ba(Zr_{0.2}Ti_{0.8})O_3$-0.5$(Ba_{0.7}Ca_{0.3})TiO_3$ using convergent beam electron diffraction method," J. Appl. Phys. **115**, 054108 (2014).
[23]M. C. Ehmke, S. N. Ehrlich, J. E. Blendell, and K. J. Bowman, "Phase coexistence and ferroelastic texture in high strain (1-x)$Ba(Zr_{0.2}Ti_{0.8})O_3$-x$(Ba_{0.7}Ca_{0.3})TiO_3$ piezoceramics," J. Appl. Phys. **111**, 124110 (2012).
[24]D. Xue, Y. Zhou, H. Bao, J. Gao, C. Zhou, and X. Ren, "Large piezoelectric effect in Pb-free Ba(Ti, Sn)O_3-x(Ba, Ca)TiO_3 ceramics," Appl. Phys. Lett. **99**, 122901 (2011).
[25]C. Zhou, W. Liu, D. Xue, X. Ren, H. Bao, J. Gao, and L. Zhang, "Triple-point-type morphotropic phase boundary based large piezoelectric Pb-free material–$Ba(Ti_{0.8}Hf_{0.2})O_3$-$(Ba_{0.7}Ca_{0.3})TiO_3$," Appl. Phys. Lett. **100**, 222910 (2012).
[26]S.-W. Zhang, H. Zhang, B.-P. Zhang, and S. Yang, "Phase-transition behavior and piezoelectric properties of lead-free $(Ba_{0.95}Ca_{0.05})(Ti_{1-x}Zr_x)O_3$ ceramics," J. Alloys Compd. **506**, 131–135 (2010).
[27]W. Li, Z. Xu, R. Chu, P. Fu, and G. Zang, "Piezoelectric and dielectric properties of $(Ba_{1-x}Ca_x)(Ti_{0.95}Zr_{0.05})O_3$ lead-free ceramics," J. Am. Ceram. Soc. **93**, 2942–2944 (2010).
[28]M. Sutapun, W. Vittayakorn, R. Muanghlua, and N. Vittayakorn, "High piezoelectric response in the new coexistent phase boundary of 0.87$BaTiO_3$–(0.13-x)$BaZrO_3$–x$CaTiO_3$," Mater. Des. **86**, 564–574 (2015).
[29]IEEE standard on piezoelectricity, 54 (1988).
[30]S. Zhang, E. F. Alberta, R. E. Eitel, C. A. Randall, and T. R. Shrout, "Elastic, piezoelectric, and dielectric characterization of modified $BiScO_3$-$PbTiO_3$ ceramics," IEEE Trans. Ultrason., Ferroelectr., Freq. Control **52**, 2131–2139 (2005).
[31]T. Mitsui and W. B. Westphal, "Dielectric and x-ray studies of $Ca_xBa_{1-x}TiO_3$ and $Ca_xSr_{1-x}TiO_3$," Phys. Rev. **124**, 1354–1359 (1961).
[32]Z. Yu, C. Ang, R. Guo, and A. S. Bhalla, "Piezoelectric and strain properties of $Ba(Ti_{1-x}Zr_x)O_3$ ceramics," J. Appl. Phys. **92**, 1489–1493 (2002).
[33]D. S. Keeble, F. Benabdallah, P. A. Thomas, M. Maglione, and J. Kreisel, "Revised structural phase diagram of $(Ba_{0.7}Ca_{0.3}TiO_3)$-$(BaZr_{0.2}Ti_{0.8}O_3)$," Appl. Phys. Lett. **102**, 092903 (2013).
[34]L. Zhang, M. Zhang, L. Wang, C. Zhou, Z. Zhang, Y. Yao, L. Zhang, D. Xue, X. Lou, and X. Ren, "Phase transitions and the piezoelectricity around morphotropic phase boundary in $Ba(Zr_{0.2}Ti_{0.8})O_3$-x$(Ba_{0.7}Ca_{0.3})TiO_3$ lead-free solid solution," Appl. Phys. Lett. **105**, 162908 (2014).
[35]D. Xue, J. Gao, Y. Zhou, X. Ding, J. Sun, T. Lookman, and X. Ren, "Phase transitions and phase diagram of $Ba(Zr_{0.2}Ti_{0.8})O_3$-x$(Ba_{0.7}Ca_{0.3})TiO_3$ Pb-free system by anelastic measurement," J. Appl. Phys. **117**, 124107 (2015).
[36]J. Gao, D. Xue, Y. Wang, D. Wang, L. Zhang, H. Wu, S. Guo, H. Bao, C. Zhou, W. Liu, S. Hou, G. Xiao, and X. Ren, "Microstructure basis for strong piezoelectricity in Pb-free $Ba(Zr_{0.2}Ti_{0.8})O_3$-$(Ba_{0.7}Ca_{0.3})TiO_3$ ceramics," Appl. Phys. Lett. **99**, 092901 (2011).
[37]Y. Zhang, D. Xue, H. Wu, X. Ding, T. Lookman, and X. Ren, "Adaptive ferroelectric state at morphotropic phase boundary: Coexisting tetragonal and rhombohedral phases," Acta Mater. **71**, 176–184 (2014).
[38]H. Wu, D. Xue, D. Lv, J. Gao, S. Guo, Y. Zhou, X. Ding, C. Zhou, S. Yang, Y. Yang, and X. Ren, "Microstructure at morphotropic phase boundary in $Pb(Mg_{1/3}Nb_{2/3})O_3$-$PbTiO_3$ ceramic: Coexistence of nano-scaled 110-type rhombohedral twin and 110-type tetragonal twin," J. Appl. Phys. **112**, 052004 (2012).
[39]D. Xue, Y. Zhou, J. Gao, X. Ding, and X. Ren, "A comparison between tetragonal-rhombohedral and tetragonal-orthorhombic phase boundaries on piezoelectricity enhancement," Europhys. Lett. **100**, 17010 (2012).
[40]F. Li, S. Zhang, Z. Xu, X. Wei, J. Luo, and T. R. Shrout, "Composition and phase dependence of the intrinsic and extrinsic piezoelectric activity of domain engineered (1-x)$Pb(Mg_{1/3}Nb_{2/3})O_3$-x$PbTiO_3$ crystals," J. Appl. Phys. **108**, 034106 (2010).
[41]F. Li, L. Jin, and R. Guo, "High electrostrictive coefficient Q_{33} in lead-free $Ba(Zr_{0.2}Ti_{0.8})O_3$-x$(Ba_{0.7}Ca_{0.3})TiO_3$ piezoelectric ceramics," Appl. Phys. Lett. **105**, 232903 (2014).
[42]S.-E. Park and T. R. Shrout, "Ultrahigh strain and piezoelectric behavior in relaxor based ferroelectric single crystals," J. Appl. Phys. **82**, 1804–1811 (1997).
[43]Y. Lu, D.-Y. Jeong, Z.-Y. Cheng, Q. M. Zhang, H.-S. Luo, Z.-W. Yin, and D. Viehland, "Phase transitional behavior and piezoelectric properties of the orthorhombic phase of $Pb(Mg_{1/3}Nb_{2/3})O_3$-$PbTiO_3$ single crystals," Appl. Phys. Lett. **78**, 3109–3111 (2001).
[44]J. Kuwata, K. Uchino, and S. Nomura, "Phase transitions in the $Pb(Zn_{1/3}Nb_{2/3})O_3$-$PbTiO_3$ system," Ferroelectrics **37**, 579–582 (1981).
[45]*Piezoelectricity*, edited by C. Z. Rosen, B. V. Hiremath, and R. Newnham (American Institute of Physics, New York, 1992).